JGR Space Physics

RESEARCH ARTICLE
10.1029/2020JA028169

Deriving the Magnetopause Position from the Soft X-Ray Image by Using the Tangent Fitting Approach

Tianran Sun[1], **Chi Wang**[1,2], **Hyunju K. Connor**[3], **Anders M. Jorgensen**[4], **and Steven Sembay**[5]

[1]State Key Laboratory of Space Weather, National Space Science Center, Chinese Academy of Sciences, Beijing, China, [2]College of Earth and Planetary Sciences, The University of Chinese Academy of Sciences, Beijing, China, [3]Geophysical Institute, The University of Alaska Fairbanks, Fairbanks, AK, USA, [4]Electrical Engineering Department, New Mexico Institute of Mining and Technology, Socorro, NM, USA, [5]School of Physics and Astronomy, The University of Leicester, Leicester, UK

Key Points:
- A novel method, namely, tangent fitting approach, has been proposed to derive the magnetopause position from an X-ray image
- The tangent fitting approach is validated using the simulated X-ray images from our MHD model
- This new approach is compared with others in the current arsenal of magnetopause reconstruction approaches

Correspondence to:
T. Sun and C. Wang,
trsun@swl.ac.cn;
cw@swl.ac.cn

Citation:
Sun, T., Wang, C., Connor, H. K., Jorgensen, A. M., & Sembay, S. (2020). Deriving the magnetopause position from the soft X-ray image by using the tangent fitting approach. *Journal of Geophysical Research: Space Physics*, *125*, e2020JA028169. https://doi.org/10.1029/2020JA028169

Received 1 MAY 2020
Accepted 6 JUL 2020
Accepted article online 10 AUG 2020

Abstract Imaging is one of the essential techniques to observe astronomical structures. While analyzing the observed images, it is a challenge in many scientific fields to reconstruct the 3-D structures from 2-D image(s). This report discusses this challenge in the context of reconstructing the structure of the Earth's magnetosphere from the X-ray image and presents a new technique. Specifically, it finds the optimum match of tangent directions derived from the X-ray image and the parameterized magnetopause function. We name this approach as the tangent fitting approach (TFA). TFA is further validated based on the magnetohydrodynamic (MHD) simulations of the X-ray images with different viewing geometries. TFA enables the reconstruction of the large-scale magnetopause from a single X-ray image, applicable to time-dependent situations such as cases during magnetic storms. It is also noted that TFA has a potential broader application to remote sensing data, for instance, energetic neutral atom (ENA) observations. Lastly, this new approach is compared with other magnetopause reconstruction approaches.

1. Introduction

For astronomical and space physics studies, imaging techniques provide key information for the study of large-scale structures, for instance, the imaging of coronal mass ejections (CMEs). Nevertheless, it was not realized that the Earth's magnetosheath is also luminous in the soft X-ray band until the discovery of the solar wind charge exchange (SWCX) process (Bhardwaj et al., 2007; Cravens, 1997; Lisse et al., 1996). The SWCX X-ray emission occurs when high charge state ions from the solar wind encounter and interact with neutral atoms or molecules in the geospace environment. As the plasma is hot and dense downstream of the Earth's bow shock and the neutral density is larger, the soft X-ray emissivity becomes stronger in the magnetosheath. This scenario has been confirmed by sporadic observations from astronomical satellites (Carter & Sembay, 2008; Carter et al., 2010, 2011; Fujimoto et al., 2007; Snowden et al., 2009) and investigated by numerical studies based on global magnetohydrodynamic (MHD) simulations (Connor & Carter, 2019; Robertson & Cravens, 2003; Robertson et al., 2006; Sibeck et al., 2018; Sun et al., 2015, 2019; Whittaker et al., 2016).

Considering that the SWCX X-ray emission carries information about the positions of magnetopause and bow shock, it is possible to derive the large-scale magnetopause structures from the X-ray images (Sun et al., 2019). Within this context, the Solar wind Magnetosphere Ionosphere Link Explorer (SMILE) mission has been proposed and jointly supported by the European Space Agency and the Chinese Academy of Sciences (Branduardi-Raymont et al., 2016; Wang et al., 2017). The Soft X-ray Imager (SXI) onboard SMILE has a wide field of view (FOV) and is expected to provide soft X-ray images of the large scale magnetopause near the subsolar region. SMILE will be launched into a highly elliptical orbit with high inclination angle, and the time frame for launch is around the year 2023–2024. In addition to SMILE-SXI, other imaging experiments such as the Lunar Environment heliospheric X-ray Imager (LEXI, http://sites.bu.edu/lexi/) deployed on the moon are currently under study.

With the advent of soft X-ray imaging enabling global observation of the magnetopause, it is critical to have appropriate techniques to extract information about the boundaries from the observed images, because

it is not straightforward to determine which part of the X-ray image corresponds to which part of the magnetopause. As the imaging process integrates the emissions along the line of sight (LOS), information about the distribution of emission along this dimension is lost. Therefore, it is a challenging task to derive 3-D magnetopause surface from 2-D image. Currently, two techniques have been developed, and each one has its own scope of application.

One of the techniques is presented by Jorgensen, Sun, Wang, Dai, Sembay, Wei, et al. (2019) and Jorgensen, Sun, Wang, Dai, Sembay, Zheng, et al. (2019), and we refer to it here as the boundary fitting approach (BFA). Based on the MHD simulation results, they first assumed some parameterized descriptions of the magnetopause and bow shock locations as well as the X-ray emissivity distribution function in the magnetosheath. Then they varied the parameters in a nonlinear fitting scheme and generated an ensemble of simulated images. These simulated images were compared with the "observed" image (as there is no satellite observation so far, the "observed" image is obtained by directly integrating the X-ray emissivity in the simulation model along the LOS), in order to find an optimal match of the X-ray intensities at each pixel inside the FOV. The parameters corresponding to the optimal match, along with the assumed functions, define the reconstructed magnetopause position. This technique makes it possible to derive the 3-D magnetopause from a single image, applicable even to events under fast solar wind variations. Nevertheless, Jorgensen, Sun, Wang, Dai, Sembay, Zheng, et al. (2019) also mentioned that the initial guess should be carefully chosen to avoid false minima in the fitting procedure. Therefore, the BFA is applicable to situations where simultaneous solar wind observations are available while imaging the magnetopause, which helps in obtaining a reasonable initial guess based on models.

The other technique is given by Collier and Connor (2018), named as the tangential direction approach (TDA). The magnetopause location can be determined by the derivative of the spacecraft position with respect to the angle of the tangent direction. By analyzing global MHD simulation runs under low and high solar wind fluxes, respectively, they concluded that the peak of the X-ray intensity corresponds to the tangential direction of the magnetopause. Given that the knowledge of the tangent direction is not sufficient to pinpoint the tangent point, further analytical derivation showed that two images observed from adjacent points can be used to derive the tangent point of the magnetopause. As it is necessary that the magnetopause remains unchanged while obtaining the two images, TDA is applicable when solar wind conditions are steady.

It is important to develop a technique applicable to cases during nonsteady solar wind conditions without solar wind observations in the vicinity of the bow shock. These situations can be more common as SMILE will be downstream of the bow shock for a majority of its orbit time without solar wind detections and pivotal for space weather studies as the geomagnetic activities often occur during solar eruptions. The tangent fitting approach (TFA) presented in section 2 enables the reconstruction of the 3-D magnetopause from a single X-ray image without prior knowledge of the solar wind conditions. We use the MHD simulation to validate this reconstruction algorithm in section 3. Lastly, the discussion about this new approach along with others in the current arsenal of magnetopause reconstruction approaches will be presented in section 4.

2. Methodology

The main idea of TFA is to compare a set of modeled tangent directions with the observed ones in order to obtain the optimum match.

2.1. TFA

Figure 1 presents the flow diagram for the TFA procedure. Assume that there is a soft X-ray image of the magnetosheath, observed by a hypothetical X-ray telescope. First, we find out the locations with maximum X-ray intensity on the image. According to the study by Collier and Connor (2018), these locations correspond to the tangent directions of the magnetopause. Then a suitable model for the magnetopause locations has been chosen, providing a parametric description of the magnetopause. Here, a modified Shue et al. (1997) model is used (refer to section 3.1 of Jorgensen, Sun, Wang, Dai, Sembay, Wei, et al., 2019 for more details), which takes into account the asymmetry of the magnetopause along the y and z axes of the GSM coordinate,

$$r(\theta,\phi)=\frac{r_y(\theta)\,r_z(\theta)}{\sqrt{\left[r_z(\theta)\cos\phi\right]^2+\left[r_y(\theta)\sin\phi\right]^2}}, \tag{1}$$

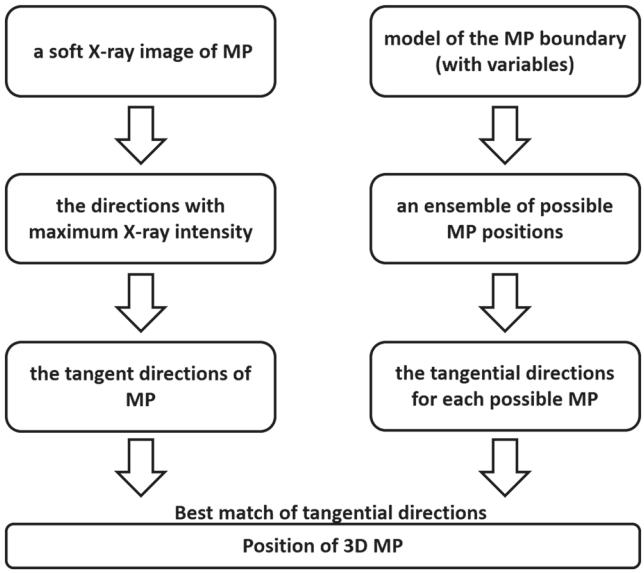

Figure 1. Flow diagram for TFA, showing the procedure to derive 3-D magnetopause (MP) position from an X-ray image.

where θ is the angle between $\vec{r}$ and the x axis, and ϕ is the angle between the y axis and the projection of $\vec{r}$ to the y-z plane. In the equation, r_y and r_z are

$$r_y(\theta) = r_0\left(\frac{2}{1+\cos\theta}\right)^{\alpha_y} \tag{2}$$

and

$$r_z(\theta) = r_0\left(\frac{2}{1+\cos\theta}\right)^{\alpha_z}, \tag{3}$$

where r_0 is the standoff distance, and the level of tail flaring on the x-y and x-z plane is represented by α_y and α_z, respectively. We vary the three variables r_0, α_y, and α_z and obtain a set of possible magnetopause profiles. For each parameter combination, the tangent directions of the magnetopause as seen by the telescope are calculated. Finally, these tangent directions for the set of magnetopause positions are compared with those derived from the observed X-ray image. The optimal match of the tangent directions corresponds to the parameters that define the reconstructed magnetopause. More sophisticated magnetopause models can be further tested in future work, but as will be shown later in the next section, the reconstructed magnetopause based on this model closely matches the MHD results. Thus, the three parameters r_0, α_y, and α_z in this model are sufficient to represent the large-scale morphology of the magnetopause.

2.2. MHD Simulation

To test the validity of TFA, the PPMLR-MHD code (Hu et al., 2007) is used to produce the X-ray image in this study. The code employs the piecewise parabolic method to provide the MHD description of the solar wind-magnetosphere-ionosphere system in the GSM coordinate. For the studied simulation run, the solar wind conditions are $V_x = 400$ km/s, $N = 22.5$ cm^{-3}, and $B_z = 5$ nT, and the spatial resolution is $0.1\,R_E$ inside the cube with $-10 \le x,y,z \le 10\,R_E$ and gradually decreases outside (the same data set was used by Jorgensen, Sun, Wang, Dai, Sembay, Wei, et al., 2019). The PPMLR-MHD code provides the plasma parameters in the geospace environment, such as the number density and bulk velocity of the solar wind plasma, as well as the thermal velocity (n_{sw}, u_{sw}, and u_{th}). Then the X-ray intensity along a specific LOS is calculated by the integration of the X-ray emissivity P_X in that direction:

$$I_X = \frac{1}{4\pi}\int P_X dr = \frac{1}{4\pi}\int \alpha_X n_H n_{sw}\sqrt{u_{sw}^2 + u_{th}^2}\,dr \quad (keV\ cm^{-2}\ s^{-1}\ sr^{-1}), \tag{4}$$

where α_X is the interaction efficiency factor, approximated by 10^{-15} eV cm^2 as also used in the paper Jorgensen, Sun, Wang, Dai, Sembay, Wei, et al. (2019), and the exospheric hydrogen density is described by $n_H = 25(10R_E/r)^3$ cm^{-3} following Cravens et al. (2001). It is noted that for the calculation of I_X, the plasma

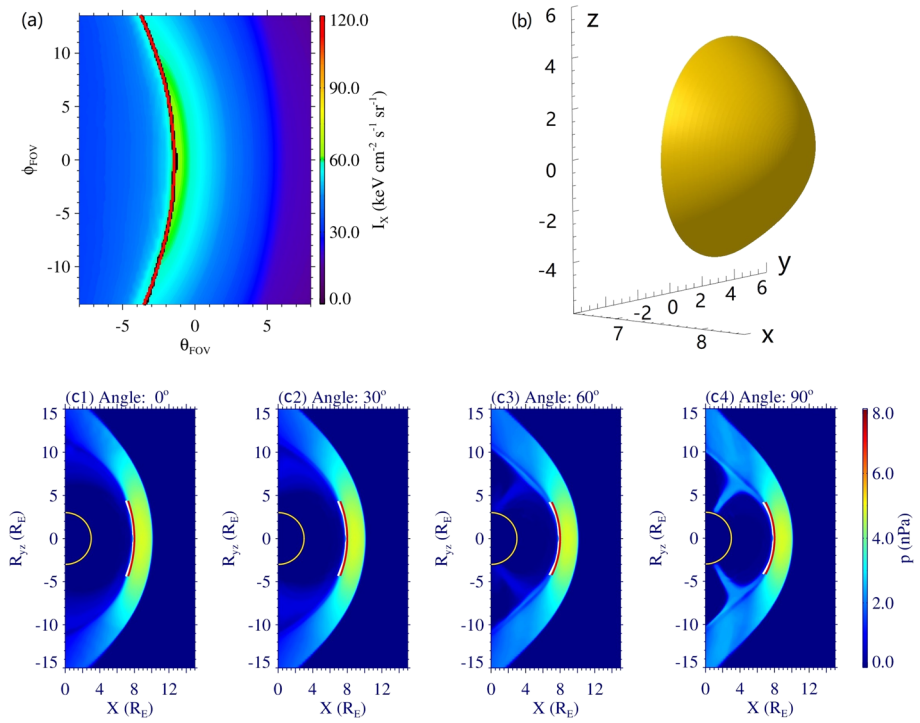

Figure 2. Reconstructed magnetopause. (a) Simulated X-ray image inside the FOV. The black curve is tangent directions indicated by max(I_X), and the red curve shows the best match calculated from the parameterized function. (b) Reconstructed 3-D magnetopause. (c1–c4) Contours of plasma thermal pressure on different planes rotating around the x axis by 0°, 30°, 60°, and 90° respectively, starting at the equatorial plane. The white and red curves show the MHD magnetopause and the reconstructed one, respectively.

number density inside the magnetopause is set to zero to avoid magnetospheric brightening, as the SWCX emission is considered to be negligible in the magnetosphere. The MHD magnetopause is basically determined based on the flux method; that is, as the plasma flux sharply decreases from the magnetosheath to the magnetosphere, the place where the plasma flux decrease to half of the solar wind level is defined as the magnetopause position. In close vicinity of the subsolar magnetopause where the plasma velocity is very small, the gradient of number density is also considered to modulate the magnetopause position.

Combining the X-ray intensity along each LOS inside the FOV, the soft X-ray image can be obtained. In the following section, we will analyze the image and use TFA to reconstruct the magnetopause.

3. Reconstruction Results

In this section, a hypothetical X-ray telescope is assumed to observe the magnetosheath from one typical vantage point (section 3.1) and then a succession of points on a designed SMILE orbit (section 3.2). The X-ray images are then obtained from the MHD simulation results by using the method described in section 2.2. From these images, reconstruction results using the TFA will be presented to validate the method from different viewing geometries.

3.1. Reconstruction From a Typical Image

The point at (5.33, 0.93, 18.93) R_E in the GSM coordinate is chosen as representative of typical positions near the apogee of the designed SMILE orbit. An idealized telescope is assumed to image the magnetosheath from this location, pointing toward the target point (8.5, 0.0, 0.0) R_E, which is close to the subsolar magnetopause. The FOV is the same with SMILE-SXI, which is $16 \times 27°$. Figure 2a shows the X-ray intensity inside the FOV. In the $\theta_{FOV} - \phi_{FOV}$ coordinate, (0, 0) corresponds to the direction pointing to the target point, and the positive θ_{FOV} axis is oriented toward the Sun. This is the soft X-ray image expected to be observed by the idealized telescope, from which we start the reconstruction of magnetopause.

The black curve in Figure 2a depicts the positions with maximum X-ray intensity along the θ_{FOV} direction for each fixed ϕ_{FOV} value. This indicates the tangent directions of the magnetopause according to Collier and Connor (2018). Equations 1–3 portray the magnetopause profile with three variables r_0, α_y, and α_z. These variables are varied within their reasonable ranges: 6–10 R_E for r_0 in 0.1 R_E steps and 0–1 for α_y and α_z in 0.05 steps. Tangent directions for the set of magnetopause morphologies are numerically calculated and recorded while looping over all the possible values of r_0, α_y, and α_z. As the number of variables are limited to 3 in this study, it is feasible to use the algorithm such that every point in the search space is visited, so that the possible false minima caused by an inaccurate initial guess can be successfully avoided (Jorgensen, Sun, Wang, Dai, Sembay, Zheng, et al., 2019). These tangent directions are compared with those derived from the X-ray image, that is, the black curve in Figure 2a. Finally, the reconstructed magnetopause is defined by the parameters corresponding to the optimal match of the tangent directions, shown by the red curve in Figure 2a: $r_0 = 8.0R_E$, $\alpha_y = 0.8$, and $\alpha_z = 0.2$. The standard deviation between the black and red curves, that is, the error, is 0.07°. These derived values for the three parameters, along with Equations 1–3, are able to portray the whole reconstructed magnetopause. But it is noted that as expected, the accuracy of the reconstruction result is higher in the subsolar region covered by the X-ray observation of SMILE-SXI and lower toward the flanks and tail of the magnetopause where the instrument FOV does not cover. Therefore, we only focus on the region around the subsolar magnetopause to compare the reconstructed result with MHD as follows.

To better evaluate the reconstruction result, Equation 1 is used to directly fit the MHD magnetopause. FOV of the X-ray image in Figure 2a is $16 \times 27°$, which roughly corresponds to the region with $\theta \leq 32°$ in the equatorial plane with this viewing geometry (θ is defined in Equation 1). Therefore, the part of magnetopause with $\theta \leq 32°$ is used to fit and obtain the parameters for the "truth": $r_0 = 7.9R_E$, $\alpha_y = 0.6$, and $\alpha_z = 0.1$. By comparison, it is seen that the reconstructed standoff distance r_0 matches well with the MHD result, and α_y and α_z also give a reasonable description of the magnetopause flaring. The 3-D view of the reconstructed magnetopause by using TFA is illustrated in Figure 2b, with $\theta \leq 32°$.

Figures 2c1–2c4 depict the MHD magnetopause and reconstructed result by the white and red curves, respectively. Contours of thermal pressure are plotted on different planes rotating with respect to the x axis, with Figure 2c1 showing the equatorial plane and Figure 2c4 showing the noon-midnight meridian plane. Only the part of magnetopause with $\theta \leq 32°$ is marked in the figure, for the reason already discussed above. It can be seen in Figure 2b that the reconstructed magnetopause is in good agreement with the MHD boundary, especially near the subsolar region. The deviation becomes slightly larger toward the flanks, where the reconstructed magnetopause is at slightly larger radius than the MHD boundary. This deviation is 0.21, 0.22, 0.24, and 0.26 R_E at $\theta = 32°$ in the four planes, Figures 2c1–2c4, respectively. Actually, the magnetopause is a layer in the MHD simulation instead of a sharp boundary, mainly due to numerical dissipation. The direction with maximum X-ray intensity better indicates the outer boundary of this layer (Sun et al., 2019), while the MHD magnetopause shown by the white curves in this study is closer to the center of this transition region. Consequently, the red curves derived from maximum X-ray intensity are expected to be at slightly larger radius, and the deviation becomes larger with increasing θ as the boundary layer becomes thicker.

As mentioned by Sun et al. (2019), the direction with maximum X-ray intensity ($\max(I_X)$) better indicates the outer boundary of the magnetopause transition layer, and the direction with maximum gradient of the X-ray intensity ($\max(dI_X)$) mainly corresponds to the center. As a result, if the tangent direction is calculated by finding the location with $\max(dI_X)$ instead of $\max(I_X)$, the reconstructed magnetopause is expected to have a slightly smaller scale. Considering this, TFA is also tested using $\max(dI_X)$, and the results are $r_0 = 7.9R_E$, $\alpha_y = 0.6$, and $\alpha_z = 0.2$. Here, values of r_0 and α_y are slightly smaller than the previous result based on $\max(I_X)$. This indicates a slightly smaller radius of the magnetopause and thus better compliance with the MHD profile, consistent with the above discussion. It is noted that while analyzing real satellite data, the difference between $\max(dI_X)$ and $\max(I_X)$ directions could be subtle as the width of the boundary layer near the subsolar point is less than several hundreds of kilometers according to in situ observations. And even in MHD studies with unavoidable numerical dissipation, the difference caused by using TFA based on $\max(dI_X)$ and $\max(I_X)$ is not significant near the subsolar point, comparable to the numerical grid spacing.

3.2. Reconstructions Along One Orbit

Successive sampling points during an apogee pass have been selected to study whether the technique is independent of the satellite location. The left panel of Figure 3 shows the candidate orbit for SMILE and

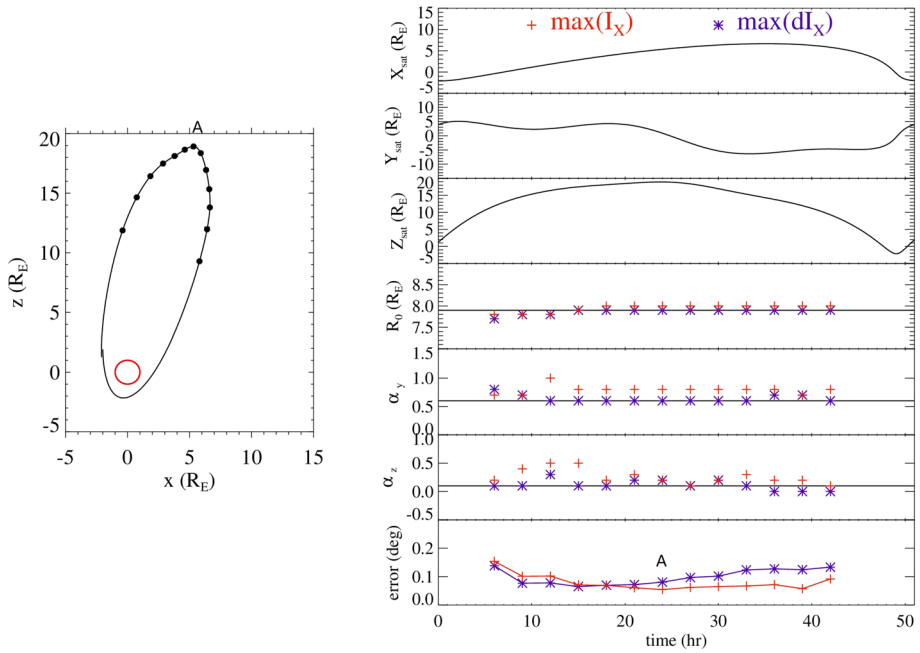

Figure 3. Reconstructed parameters from vantage points along one orbit. The left panel is the plot of the orbit. Right panels show satellite positions on the $x/y/z$ axes, $r_0/\alpha_y/\alpha_z$ obtained by applying TFA, and the error from top to bottom. The horizontal lines in the fourth to sixth panels mark the MHD results. Red crosses and blue stars are results based on max(I_X) and max(dI_X), respectively.

the sampling points, with the vantage point studied in section 3.1 marked by Point A. The orbit is plotted in the GSM coordinate, as all the MHD results in the paper are presented in GSM. Starting from the same point in section 3.1 near apogee, we trace forward and backward along the orbit and record the satellite position every 2 hr. The sampling process stops right before the satellite enters the magnetosphere, where the TFA becomes invalid as it is not able to make a tangent direction from an interior point. The position of the satellite, as a function of time, is shown in the top three panels of Figure 3. The fourth to sixth panels show the reconstructed parameters at the corresponding sampling points, with the red crosses and blue stars marking the results using TFA based on max(I_X) and max(dI_X), respectively. The horizontal lines show the parameters obtained by directly fitting the magnetopause function to the MHD simulation results. At a majority of the sampling points, the standoff distance is accurately derived and the difference from the "true value" is no larger than 0.1 R_E, which is the spatial resolution in the MHD code. The last panel in Figure 3 shows the standard deviation of the tangent directions, and it is around 0.1°. Note that the error becomes larger when the satellite is fairly close to the magnetopause. For instance, for the viewing geometry at time = 6 hr (the leftmost dot in the left panel of Figure 3), with the satellite just outside of the high latitude magnetopause, the reconstructed R_0 is smaller than the MHD result. This is expected if we consider the extreme when the satellite is right on the magnetopause. Under this situation, the satellite is located on the tangential plane, and consequently, the reconstructed magnetopause degenerates into a single point, that is, that tangential point.

4. Discussion

For any kinds of imaging processes, loss of information due to the LOS integration is inevitable. Therefore, it is unlikely to derive the 3-D configuration from a single 2-D image without making any hypotheses. If the reconstruction process is performed based on a set of images, it is possible that very few or no assumptions are required, on the condition that this set of images is taken for the same magnetopause profile. If the magnetopause profile changes significantly, reconstruction techniques based on a single image is inevitable. In this case, however, reasonable assumptions are required.

In this report, TFA is proposed to derive the 3-D magnetopause from a single image, and two assumptions are made, that is, the functional form of magnetopause as well as the conclusion that maximum X-ray intensity

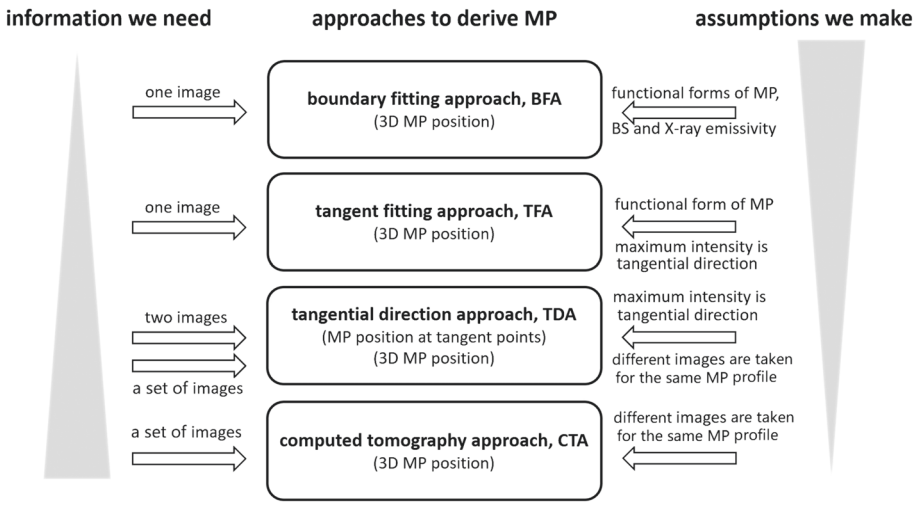

Figure 4. Current arsenal of reconstruction techniques.

indicates the tangent direction. For the first assumption, a modified Shue model (Shue et al., 1997) is used. The Shue model is a popular empirical model based on in situ satellite observations mostly at low latitudes, which assumes a rotational symmetric magnetopause. In reality, magnetic reconnections occurring on the magnetopause lead to asymmetry on the *x*-*y* and *x*-*z* plane, which can be revealed by the modified Shue model in this report. As shown in Figure 2, the modified Shue model is a good representation of the magnetopause profile. The second assumption is about the tangent direction derived from the X-ray image. Collier and Connor (2018) validated it by using MHD under different solar wind conditions from various viewing geometries. Therefore, both assumptions used in TFA are reasonable.

Several approaches to reconstruct the 3-D magnetopause from the 2-D image have been developed so far, forming an arsenal of reconstruction techniques. Each approach has pros and cons, having its own scope of application. Each reconstruction technique is actually a balance between the information we need and the assumptions we make, as illustrated in Figure 4. The BFA (introduced in section 1) and TFA are conducted on the basis of a single image and thus are applicable to situations with rapid solar wind variations. Both algorithms need assumptions. The differences between the BFA and TFA are as follows. First, the TFA does not require assumptions about the shape of bow shock and the distribution of X-ray emissivity in the magnetosheath, while the BFA does. Therefore, the TFA is based on less assumptions of the structures in the magnetospheric system. This makes it applicable to situations with the presence of time-dependent phenomenons in the magnetosheath, such as waves. Second, the number of fitted parameters is reduced to 3 in the TFA, compared to the total 11 parameters in the BFA. Consequently, the greatly reduced number of free parameters in the TFA makes it feasible to avoid the possible false minima caused by an inaccurate initial guess. Therefore, unlike the BFA indicated by Jorgensen, Sun, Wang, Dai, Sembay, Zheng, et al. (2019), applying the TFA does not require simultaneous solar wind observations to provide a carefully evaluated initial guess. Third, as the TFA calculated the tangent directions of the magnetopause, it is not applicable while the satellite is inside the magnetosphere. The application of BFA does not have the restriction.

The TDA (introduced in section 1) uses two or more images to derive the tangent point or the 3-D magnetopause. The computed tomography approach (CTA) is the traditional CT approach applied to the X-ray images of magnetopause, and the relevant paper is currently in development. It analyzes a set of images and reconstructs the 3-D X-ray emissivity. The 3-D magnetopause surface can subsequently be derived from the emissivity plots. Both the TDA and CTA do not rely on functional forms of the magnetopause, bow shock, or X-ray emissivity. However, they require the set of images to be taken for the same magnetopause profile and thus not applicable to events with fast solar wind variations. Since both the TFA and TDA use the peak soft X-ray emission direction as the tangent direction to the magnetopause, they are applicable only when the vantage point is outside the magnetopause.

Finally, this report is a general description of the TFA in the context of soft X-ray imaging. It could be capable of deriving the 3-D magnetopause given a set of images anticipated to be observed by SMILE, LEXI, or

other future missions. The followed-up study is to apply the TFA to the MHD simulation of a magnetic storm event and further analyze the time variation of the reconstructed magnetopause caused by solar wind changes. It is also noted that the approach could be applied to other imaging techniques as well, for instance, energetic neutral atom (ENA) imaging. For a more realistic representation of SXI on SMILE, the accuracy of the TFA tested against instrument simulations in the presence of noise within the observed image will be the subject of a future work. As another possible topic for future study, TFA results may be used to constrain the magnetopause location before applying BFA as a second step to derive the bow shock position. The basic idea of TFA itself is potentially applicable to the derivation of the bow shock position as well, as the direction showing abrupt decrease of the X-ray intensity on the image is probably the tangent direction of the bow shock.

5. Summary

This report presents an new algorithm to reconstruct the 3-D magnetopause from a single X-ray image, namely, the TFA. It compares the tangent directions calculated from the parameterized magnetopause function with those derived from the X-ray images. Then the 3-D magnetopause is reconstructed by finding the optimum match of the tangent directions. Based on the MHD simulation of the X-ray images, TFA is validated from various viewing geometries. TFA is applicable to studies during nonsteady solar wind conditions without further requirements on simultaneous solar wind measurements. Utilizing it to analyze the images anticipated to be observed by future missions such as SMILE, it is expected to reveal the time evolutions of the large-scale magnetopause during magnetic storms and perform real-time monitoring of the magnetopause. Finally, this new approach is compared with other magnetopause reconstruction approaches, with each approach having its own scope of application.

Data Availability Statement

The data for X-ray images studied in this paper can be downloaded from Zenodo (https://doi.org/10.5281/zenodo.3751044).

Acknowledgments
The authors gratefully acknowledge Prof. Y. Q. Hu for providing information on the MHD simulation code. This work was supported by NNSFC Grants 41774173 and 41731070, Key Research Program of Frontier Sciences, CAS, Grant No. QYZDJ-SSW-JSC028, Strategic Pionner Program on Space Science, CAS, Grant Nos. XDA15052500, XDA15350201, and XDA15017000, and in part by Research Fund from the Chinese Academy of Sciences and the Specialized Research Fund for State Key Laboratories of China. Tianran Sun is also supported by the Young Elite Scientists Sponsorship Program by CAST (2017QNRC001) and the Youth Innovation Promotion Association (2016134). HC gratefully acknowledges support from NSF grants OIA-1920965 and AGS-1928883, and NASA grants 80NSSC18K1043, 80NSSC18K1052, and 80NSSC19K0844.

References

Bhardwaj, A., Elsner, R. F., Gladstone, G. R., Cravens, T. E., Lisse, C. M., Dennerl, K., et al. (2007). X-rays from solar system objects. *Planetary and Space Science*, *55*, 1135–1189.

Branduardi-Raymont, G., Escoubet, C. P., Kuntz, K., Lui, T., Read, A., Sibeck, D., et al. (2016). Link between solar wind, magnetosphere, and ionosphere. ISSI-BJ magazine, No. 9.

Carter, J. A., & Sembay, S. (2008). Identifying XMM-Newton observations affected by solar wind charge exchange—Part I. *Astronomy and Astrophysics*, *489*, 837–848.

Carter, J. A., Sembay, S., & Read, A. M. (2010). A high charge state coronal mass ejection seen through solar wind charge exchange emission as detected by XMM-Newton. *Monthly Notices of the Royal Astronomical Society*, *402*, 867.

Carter, J. A., Sembay, S., & Read, A. M. (2011). Identifying XMM-Newton observations affected by solar wind charge exchange—Part II. *Astronomy and Astrophysics*, *527*, A115.

Collier, M. R., & Connor, H. K. (2018). Magnetopause surface reconstruction from tangent vector observations. *Journal of Geophysical Research: Space Physics*, *123*, 10,189–10,199. https://doi.org/10.1029/2018JA025763

Connor, H. K., & Carter, J. A. (2019). Exospheric neutral hydrogen density at the nominal 10RE subsolar point deduced from XMM-Newton X-ray observations. *Journal of Geophysical Research: Space Physics*, *124*, 1612–1624. https://doi.org/10.1029/2018JA026187

Cravens, T. E. (1997). Comet Hyakutake X-ray source: Charge transfer of solar wind heavy ions. *Geophysical Research Letters*, *24*, 105–108.

Cravens, T. E., Robertson, I. P., & Snowden, S. L. (2001). Temporal variations of geocoronal and heliospheric X-ray emission associated with the solar wind interaction with neutrals. *Journal of Geophysical Research*, *106*(24), 883.

Fujimoto, R., Mitsuda, K., McCammon, D., Takei, Y., Bauer, M., Ishisaki, Y., et al. (2007). Evidence for solar-wind charge-exchange X-ray emission from the Earth's magnetosheath. *Publications of the Astronomical Society of Japan*, *59*, 133–140.

Hu, Y. Q., Guo, X. C., & Wang, C. (2007). On the ionospheric and reconnection potentials of the Earth: Results from global MHD simulations. *Journal of Geophysical Research*, *112*, A07215. https://doi.org/10.1029/2006JA012145

Jorgensen, A. M., Sun, T., Wang, C., Dai, L., Sembay, S., Wei, F., et al. (2019). Boundary detection in three dimensions with application to the SMILE mission: The effect of photon noise. *Journal of Geophysical Research: Space Physics*, *124*, 4365–4383. https://doi.org/10.1029/2018JA025919

Jorgensen, A. M., Sun, T., Wang, C., Dai, L., Sembay, S., Zheng, J. H., & Yu, X. Z. (2019). Boundary detection in three dimensions with application to the SMILE mission: The effect of model-fitting noise. *Journal of Geophysical Research: Space Physics*, *124*, 4341–4355. https://doi.org/10.1029/2018JA026124

Lisse, C. M., Dennerl, K., Englhauser, J., Harden, M., Marshall, F. E., Mumma, M. J., et al. (1996). Discovery of X-ray and extreme ultraviolet emission from Comet C/Hyakutake. *Science*, *274*, 205–209.

Robertson, I. P., Collier, M. R., Cravens, T. E., & Fok, M.-C. (2006). X-ray emission from the terrestrial magnetosheath including the cusps. *Journal of Geophysical Research*, *111*, A12105. https://doi.org/10.1029/2006JA011672

Robertson, I. P., & Cravens, T. E. (2003). X-ray emission from the terrestrial magnetosheath. *Geophysical Research Letters*, *30*(8), 1439. https://doi.org/10.1029/2002GL016740

Shue, J.-H., Chao, J., Fu, H., Russell, C., Song, P., Khurana, K., & Singer, H. (1997). A new functional form to study the solar wind control of the magnetopause size and shape. *Journal of Geophysical Research*, *102*, 9497–9511.

Sibeck, D. G., Allen, R., Aryan, H., Bodewits, D., Brandt, P., Branduardi-Raymont, G., et al. (2018). Imaging plasma density structures in the soft X-rays generated by solar wind charge exchange with neutrals. *Space Science Reviews*, *214*, 79. https://doi.org/10.1007/s11214-018-0504-7

Snowden, S. L., Collier, M. R., Cravens, T., Kuntz, K. D., Lepri, S. T., Robertson, I., & Tomas, L. (2009). Observation of solar wind charge exchange emission from exospheric material in and outside Earth's magnetosheath 2008 September 25. *The Astrophysical Journal*, *691*, 372–381.

Sun, T. R., Wang, C., Sembay, S. F., Lopez, R. E., Escoubet, C. P., Branduardi-Raymont, G., et al. (2019). Soft X-ray imaging of the magnetosheath and cusps under different solar wind conditions: MHD simulations. *Journal of Geophysical Research: Space Physics*, *124*, 2435–2450. https://doi.org/10.1029/2018JA026093

Sun, T. R., Wang, C., Wei, F., & Sembay, S. (2015). X-ray imaging of Kelvin-Helmholtz waves at the magnetopause. *Journal of Geophysical Research: Space Physics*, *120*, 266–275. https://doi.org/10.1002/2014JA020497

Wang, C., Li, Z. J., Sun, T. R., Liu, Z. Q., Liu, J., Wu, Q., et al. (2017). SMILE Satellite mission survey. *Space International (in Chinese)*, *464*, 13–16.

Whittaker, I. C., Sembay, S., Carter, J. A., Read, A. M., Milan, S. E., & Palmroth, M. (2016). Modeling the magnetospheric X-ray emission from solar wind charge exchange with verification from XMM-Newton observations. *Journal of Geophysical Research: Space Physics*, *121*, 4158–4179. https://doi.org/10.1002/2015JA022292